

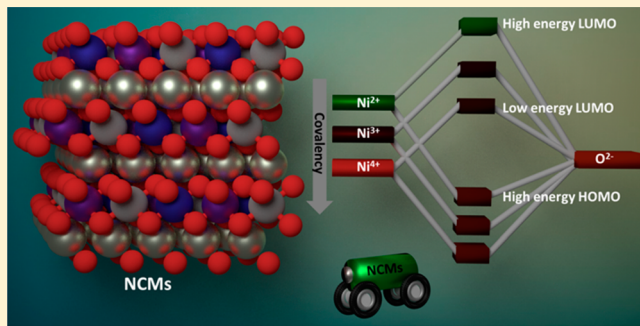
Origin of Structural Degradation During Cycling and Low Thermal Stability of Ni-Rich Layered Transition Metal-Based Electrode Materials

Mudit Dixit,[†] Boris Markovsky,[†] Florian Schipper,[†] Doron Aurbach,[†] and Dan T. Major^{*,†}

[†]Department of Chemistry and the Lise Meitner-Minerva Center of Computational Quantum Chemistry, Bar-Ilan University, Ramat-Gan 52900, Israel

Supporting Information

ABSTRACT: Ni-rich lithiated layered oxides composed of Ni, Co, and Mn (NCMs) have shown tremendous promise as cathode materials in lithium-ion batteries (LIB) for electromobility applications. The capacity of these materials increases with nickel content, but there is a concomitant decrease in stability and stable operating voltage during cycling. Hence, it is of great importance to probe ways to increase the nickel content without sacrificing other important aspects. In this study, we performed a detailed comparative theoretical study of Ni-rich NCMs to advance our understanding of the cycling and thermal stability. On the basis of extensive analysis of density of states, magnetic structure, bond covalency, molecular orbital diagrams, Bader atomic charges, and oxygen binding energies, we draw several crucial conclusions: as the NCM materials become increasingly rich in Ni, (1) the amount of high-valence Ni-ions increases (i.e., Ni^{3+} , Ni^{4+}), (2) Ni^{4+} ions are readily reduced due to a low-lying LUMO, and hence can easily react with electrolyte species, (3) Ni^{4+} -O bonds become increasingly covalent, and (4) molecular oxygen release becomes more feasible and, hence, may result in cathode degradation. Importantly, these conclusions are found to be appropriate also for the deintercalation process for all NCM materials and therefore also explain cycling behavior. On the basis of the current results, we suggest that a strategy of doping NCMs with high-valent cations, which suppresses Ni-ions in high oxidation states via charge compensation, should be adopted. These results will be beneficial for understanding and designing high capacity LIB cathodes for electric vehicles.



1. INTRODUCTION

The excellent performance of lithium ion batteries (LIB) has led to a revolution in portable electronic devices, and nowadays LIBs are empowering electric vehicles (EVs).¹ Among the various factors influencing the performance of LIBs, the positive electrode (cathode) material is arguably the most important component, as the nature of the cathode primarily controls the capacity and the stability of LIBs.^{2–10}

Recently, lithiated transition metal (TM) oxides of the form $\text{Li}[\text{Ni}_x\text{Co}_y\text{Mn}_z]\text{O}_2$ (i.e., NCM) emerged as a very promising family of cathode materials for LIB, and one of these materials NCM-333 ($\text{LiNi}_{0.33}\text{Co}_{0.33}\text{Mn}_{0.33}\text{O}_2$) is already commercialized.¹¹ However, NCM-333 cannot be used in next generation EV applications due to its low capacity (155 mAh g^{-1}).⁸ The growing demand for high-energy density materials has led to tremendous research efforts in a quest to discover novel NCM compositions. Among the family of NCM materials, the Ni-rich materials (i.e., $x > 0.5$) have shown to be high energy-density, low cost alternatives to LiCoO_2 .¹² Indeed, the capacity of layered NCM materials grows linearly with increasing Ni content, while the stability decreases with Ni content.^{13,14}

The thermal stability of cathode materials, especially in the delithiated state at voltages $\geq 4.3 \text{ V}$, is a major safety concern for

practical applications and therefore should be addressed carefully. To design high capacity NCM-based cathode materials with enhanced stability, it is important to understand the capacity-stability trade-off in Ni-rich NCM materials. Notably, the practical capacities ($\sim 200 \text{ mAh g}^{-1}$ for NCM-811, $\sim 4.3 \text{ V}$) of Ni-rich NCMs are significantly lower in comparison to their theoretical capacity (278 mAh g^{-1} for NCM-811).¹⁴ In principle, higher practical capacities could be obtained at higher voltages; however, at high voltages the instabilities of Ni-rich NCMs become a serious concern. Indeed, at high voltages drastic capacity degradation and rise in impedance during cycling have been reported.¹⁴

The reasons for the reduced thermal and cycling stability of NCMs with Ni content are not fully understood, yet. It has been established that TM in different oxidation states can modulate features of cathode materials. For instance, Mn^{4+} and Co^{3+} stabilize the NCM structure, while Ni^{3+} and Mn^{3+} show Jahn-Teller distortions.^{14–19} Ni^{2+} and Mn^{2+} ions may undergo interlayer migrations at high voltages, which can lead to phase

Received: June 22, 2017

Revised: September 10, 2017

Published: September 22, 2017

transitions.^{20–22} Previously, various studies proposed different factors influencing the thermal and cycling stability of Ni-rich materials. Several studies suggested that the observed instabilities of Ni-rich materials are mainly due to high concentration of unstable Ni^{4+} ions in partially delithiated states and that these ions tend to reduce to the Ni^{2+} state with oxygen loss.^{16,18,23,24}

Sun and co-workers recently studied the structural and electrochemical properties of different NCMs.¹⁶ They suggested that the instability of partially delithiated states increases with Ni content due to the presence of Ni^{4+} ions. Hwang et al. studied the thermal stability of different NCMs and found that the onset temperature of both oxygen release and phase transitions decreases with increasing amounts of Ni.¹⁸ They further suggested that the oxygen release is associated with cation migration leading to irreversible phase transitions. Previously, Bruce and co-workers demonstrated that in the Li-rich material $\text{Li}[\text{Ni}_{0.2}\text{Li}_{0.7}\text{Mn}_{0.6}]_{\text{O}_2}$ oxygen evolution occurs on charge beyond 4.5 V,¹⁷ and these authors also proposed that oxygen evolution is associated with TM migrations. Tarascon and co-workers have established that there is a fundamental relation between anionic redox and oxygen bond formation in layered oxides.^{25,26}

Another aspect of Ni-rich materials is the pronounced cation mixing (cation disorder) that occurs during cycling. The effect of this mixing is currently debated, and no consensus has been reached whether cation mixing is beneficial for performance or whether it leads to capacity degradation.¹⁴ However, it has been established that in Ni-rich NCMs, Ni acts as a charge modulator and as the main redox center, whereas Mn and Co serve to stabilize these materials.^{14,18,19,27}

Various approaches have been suggested to improve cycling stability and enhance the thermal behavior of Ni-rich NCM materials.^{28–34} These approaches include lattice cationic and anionic doping, core–shell cathode materials with reduced Ni-content in the shell, and coatings of cathode materials by thin surface layers (e.g., oxides or salts). The latter approaches can protect the materials from side reactions with solution species and substantial increase the thermal stability of NCMs in the delithiated state.

To answer the intriguing question of instability of Ni-rich materials, it is important to examine and compare the electronic structure of NCM materials at different Ni concentrations. In this study, we employ density functional theory (DFT) to perform a comparative analysis of the electronic structure, structural details, chemical bonding, and oxygen vacancy formation of different NCMs (NCM-424, NCM-523, NCM-622, and NCM-811) at varying levels of lithiation. This work complements the recent work of Sun and Zhao, which addressed the mechanical properties and electronic structure of pristine NCM materials.³⁵ On the basis of the current findings, we suggest a practical strategy to reduce the oxidation state of Ni-ions by high-valent cation doping and thus improve the stability and performance of Ni-rich layered materials.

2. COMPUTATIONAL METHODS

All DFT calculations were performed with the Vienna ab initio simulation package^{36–38} (VASP) with antiferromagnetic spin ordering, as suggested by previous studies.^{39–41} The generalized gradient approximation (GGA) PBE exchange-correlation functional⁴² with the plane-wave projector augmented wave method was used for all calculations. The kinetic energy cutoff was set to 520 eV for all calculations.

The electronic structure (relative positions of the TM d- and oxygen p-states) of layered LiTMO_2 -type materials predicted by the PBE method often shows good agreement with the experimental electronic structure,^{43–45} despite the inherent self-interaction of PBE. Moreover, PBE accurately predicts the intercalation voltage trends, defects, and interlayer stacking of layered TM oxide materials.^{15,22,27,46–49} One can add Hubbard correction parameters (U) to PBE to correct for the self-interaction error, although this can perturb the electronic structure. Unfortunately, the optimal value of the U parameter is dependent on the degree of electron correlation, and in layered LiTMO_2 -based materials, the electron correlation varies with the level of lithiation (i.e., oxidation state of TMs).^{50,51} Previously, it was demonstrated that for LiTMO_2 system, the U values that give correct electronic structure (for LiCoO_2 $U \sim 2.9$ eV and for LiNiO_2 $U \sim 4.0$ eV) could not predict accurate voltages, and hence higher U values (for LiCoO_2 $U \sim 4.9$ eV and for LiNiO_2 $U \sim 6.4$ eV) are often chosen to compute the average voltage.^{52–54} However, adding U corrections to the PBE functional gives incorrect voltage profiles (i.e. trends),^{27,47} and hence we chose to use PBE without any Hubbard correction. Dispersion corrections were included via the opt-PBE-vdW functional.⁵⁵

The geometries were considered minimized when the maximum force was found to be less than 0.01 eV/atom. The NCM system were constructed using a supercell of 5×4 (60 formula units, $R\bar{3}m$ space group) of an $\alpha\text{-NaFeO}_2$ -type structure. Due to considerations of computational costs (240 atoms), all calculations were performed with the gamma k -point only.

Additionally, we have also performed chemical-bonding analysis by plotting the crystal orbital Hamiltonian population (COHP).^{56–58} This scheme has been implemented in the LOBSTER program, which calculates COHPs directly from the plane-wave output.⁵⁸

Binding energies for molecular oxygen ($\Delta E_{\text{O}_2}^{\text{bind}}$) for NCMs were computed using the following equation:

$$\Delta E_{\text{O}_2}^{\text{bind}} = E(\text{NCM}_{\text{defective}}) + E_{\text{O}_2} - E(\text{NCM}_{\text{perfect}}) \quad (1)$$

where $E(\text{NCM}_{\text{defective}})$ represents the total energy of the system with two neighboring oxygen vacancies, $E(\text{NCM}_{\text{perfect}})$ represents the total energy of the NCM system without any oxygen vacancies, and E_{O_2} represents the energy of a gaseous O_2 molecule (modeled as a single molecule in a large periodic box). To compute the energy of O_2 -defect structures for the calculation of oxygen molecular binding energies, the oxygen molecule with the shortest O–O distance was removed from the supercell. Several defect candidates with close O–O distances were considered and the lowest energy defect structures were considered for oxygen binding energy calculations.

3. RESULTS AND DISCUSSION

3.1. Structure of NCM Materials during Cycling.

Lithiated layered oxides of Ni, Co, and Mn (NCMs) exhibit preferential TM orderings, which are thought to be governed by electrostatic interactions.⁵⁹ Several experimental reports have identified a $(\sqrt{3} \times \sqrt{3})R30$ type of ordering in NCMs.^{60–64} To predict low-energy cationic ordering in NCM materials, we prescreened various $\sqrt{3}$ -ordering structures using DFT calculations, and the lowest energy structures were considered for further calculations. The NCM structures

with the most stable cationic orderings were fully relaxed at different Li-compositions with various Li arrangements. To obtain the optimal Li-orderings, several Li-vacancy arrangements were created manually and the lowest energy arrangements were considered at every composition. We note that in the most stable structures, the Li ions were found to be ordered with large Li–Li separations to minimize the electrostatic repulsion.

Figure 1 shows the cationic ordering of a low energy structure of NCM-811, while the structures of NCM-424,

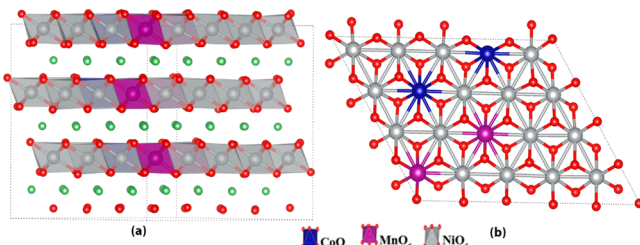


Figure 1. (a) Supercell of $\text{LiNi}_{0.8}\text{Co}_{0.1}\text{Mn}_{0.1}\text{O}_2$, in which Li atoms are marked in green; (b) most preferred cation ordering.

NCM-523, and NCM-622 are given in Figure S1. The changes in the c lattice parameter of the studied NCMs are given in Figure 2. We note significant changes in the c lattice parameter

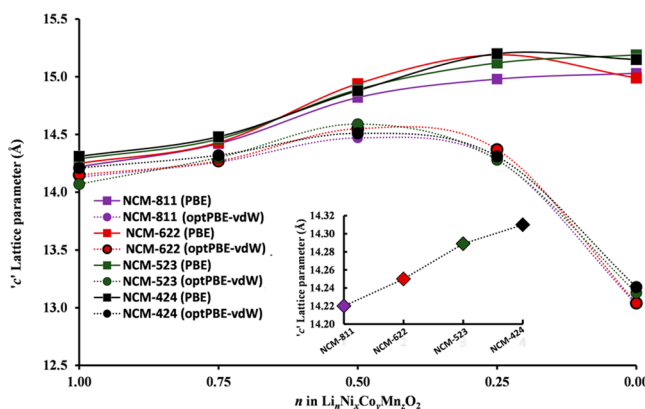


Figure 2. Change in the c lattice parameter as a function of delithiation (n) for various NCM materials using the PBE and dispersion-corrected PBE functionals. Inset figure shows the c lattice parameters of different NCMs calculated using PBE.

with the Li deintercalation, but only minor changes in the a lattice parameters were observed (Table S3). Due to the absence of dispersion, GGA methods typically predict a monotonically increasing trend for the c lattice parameter as a function of Li deintercalation.^{27,65} However, it is experimentally demonstrated that the c lattice parameter initially increases with Li-deintercalation and subsequently decreases at low Li content (Figure 2).^{23,66–69} At low lithiation levels, the metal oxide layers are separated by dilute Li-ion layers, and at this low lithiation level, weak interlayer dispersive interactions are important. Because of this, the PBE functional, which does not treat dispersion interactions well, overestimates the c lattice parameter. Indeed, the dispersion corrected functional (opt-PBE-vdW) correctly predicts the changes in the lattice parameters in accordance with experimental results for NCMs (Figure 2).^{23,66–69} We also note that the c lattice parameters of

NCMs in the pristine state decrease from NCM-424 to NCM-811 (Figure 2, inset).

3.2. Electronic Structure and Oxidation States of Transition Metals. The local magnetic moments and projected density of states (PDOS) for the NCM materials indicate that Ni may be present in a variety of oxidation states (Ni^{2+} , Ni^{3+} , and Ni^{4+}) (Figure 3). Formally, Ni^{2+} , Ni^{3+} , and Ni^{4+} have the electronic configurations $t_{2g}^6(\downarrow\uparrow\downarrow\uparrow\downarrow\uparrow)$ $e_g^2(\uparrow\uparrow\uparrow)$, $t_{2g}^6(\downarrow\uparrow\downarrow\uparrow\downarrow\uparrow)$ $e_g^1(\uparrow\uparrow\downarrow)$, and $t_{2g}^6(\downarrow\uparrow\downarrow\uparrow\downarrow\uparrow)$ $e_g^0(\uparrow\uparrow\uparrow)$, respectively. We also note that in all our calculation for the pristine materials, the Co-ions were found to have a 3+ oxidation state. This is indicated by the absence of both exchange splitting and magnetic moment on Co, hence suggesting an electronic configuration of $t_{2g}^6(\downarrow\uparrow\downarrow\uparrow\downarrow\uparrow)$ $e_g^0(\uparrow\uparrow\uparrow)$. We also note that the valence state of Mn is 4+, with an electronic configuration of $t_{2g}^3(\downarrow\uparrow\downarrow\uparrow\downarrow)$ $e_g^0(\uparrow\uparrow\uparrow)$, and this electronic structure is invariable with Ni and Li concentration. As noted previously for NCM-523 and NCM-622,^{22,27} the frontier states close to the Fermi level consist of Ni and Co ions. Specifically, the occupied states have primarily Ni^{2+} - e_g , Ni^{3+} - e_g and Co^{3+} - t_{2g} character, whereas the unoccupied states consist mostly of Ni^{3+} - e_g states. The primary presence of Ni states near the Fermi level suggests that Ni-ions play a major role in the electrochemical redox process in NCM materials. The electronic structure also suggests that the contribution of the Ni- t_{2g} states increases with Ni concentration in NCMs (Figure 3). Inspection of the DOS also reveals that the contribution of the Ni- e_g states decreases with increasing Ni concentration as we move from NCM-424 to NCM-811 (Figure 3, blue box). Two additional noteworthy features of the DOS are the shifting of the Ni bands toward the oxygen 2p bonding bands (Figure 3, orange box) and an increase in the Ni character in the oxygen 2p-bonding peaks (Figure 3, cyan box). These observations indicate a surge in the metal–oxygen covalency with increasing Ni content. Furthermore, the band gap of different NCMs follow the trend NCM-424 > NCM-523 > NCM-622 > NCM-811. This decrease in band gap along the NCM series indicates increasing electronic conductivity with higher Ni content. We note that NCM-811 shows half metallic character resembling the behavior of LiNiO_2 .⁵⁴ Interestingly, Noh et al. have experimentally confirmed that electronic conductivity increases with increasing Ni content in NCMs.¹⁶

To understand the instability of Ni-rich materials and low stable operating voltages, we examined the changes in electronic structure of Ni-rich NCM (NCM-811) as a function of delithiation (Figure 4). Careful examination of the electronic structure suggests that the Ni-character of the oxygen 2p bands increases with decreasing Li concentration (Figure 4, cyan box). These results indicate that Ni–O covalency increases with Li deintercalation. Greater M–O covalency leads to instability and subsequent oxygen loss, since delocalized oxidation holes are formed on covalent admixtures of M–O rather than localized holes forming on the metal centers, as is the case for ionic M–O bonds.⁴⁴

The contribution of Ni^{2+} - e_g and Ni^{3+} - e_g below the Fermi level decreases from $n = 1.00$ (in $\text{Li}_n\text{Ni}_{0.8}\text{Co}_{0.1}\text{Mn}_{0.1}\text{O}_2$) to $n = 0.25$ and vanishes at $n = 0.00$. However, the Co^{3+} - t_{2g} states remain almost intact, suggesting that in NCM-811, oxidation of Co takes place after $n = 0.25$. Finally, the contribution of unoccupied Ni states (Figure 4) increases with Li deintercalation indicating oxidation of Ni.

The oxidation states of TMs are known to dictate the properties of cathode materials. Figure 5 shows the oxidation

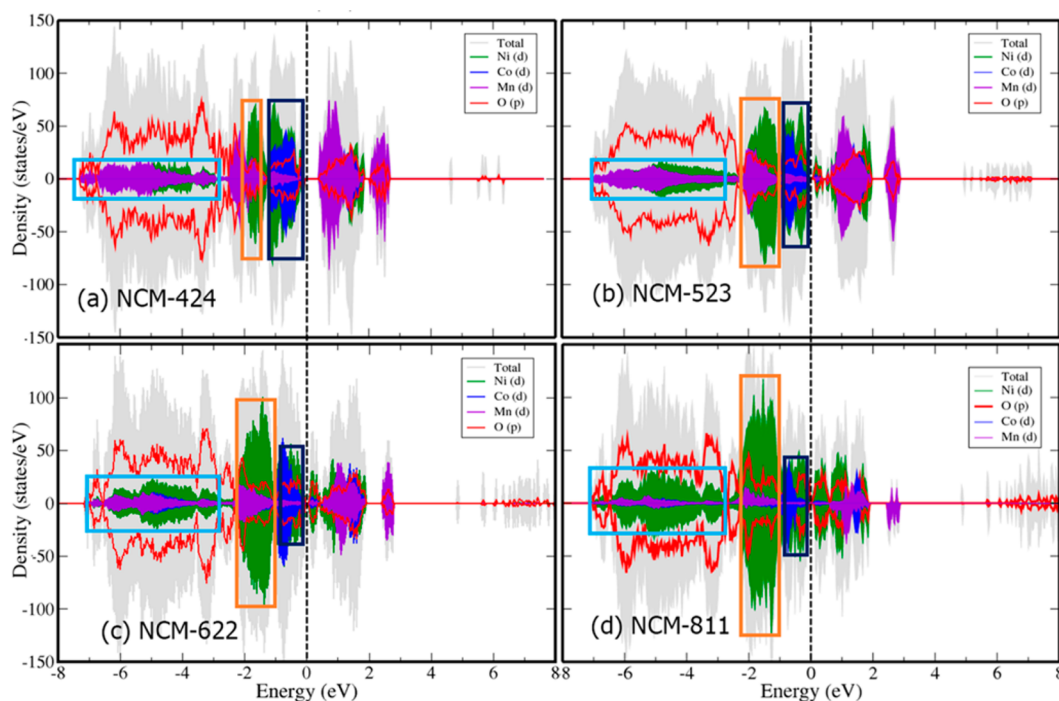


Figure 3. Density of states for (a–d) NCM-424, NCM-523, NCM-622 and NCM-811, respectively. The center, right, and left boxes indicate the Ni- t_{2g} band, Ni- e_g band, and metal character in hybridized O-metal bonding states, respectively.

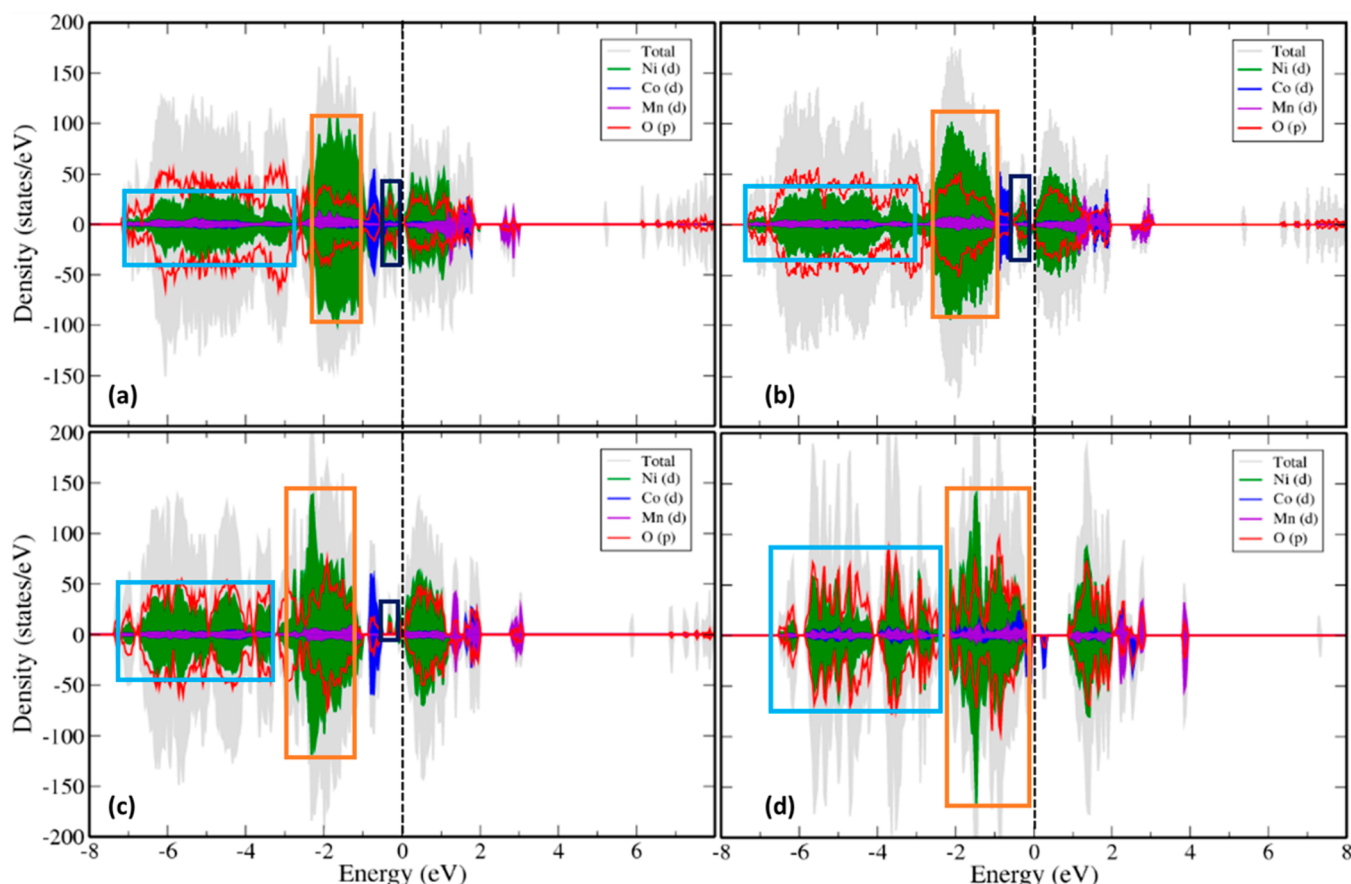


Figure 4. Density of states of NCM-811 at (a) $n = 0.75$, (b) $n = 0.50$, (c) $n = 0.25$, and (d) $n = 0.00$. The center, right, and left boxes indicate the Ni- t_{2g} band, Ni- e_g band, and metal character in hybridized O-metal bonding states, respectively.

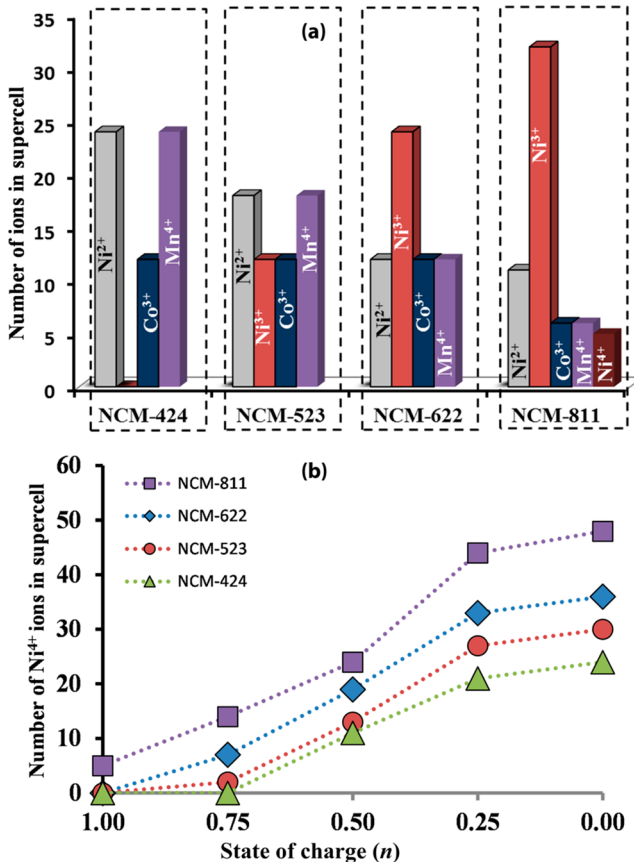


Figure 5. (a) The oxidation states of transition metal ions in various NCMs. (b) Amount of Ni⁴⁺ ions as a function of state of charge in various NCMs.

states of TMs in different pristine NCMs. The oxidation states are estimated based on the computed magnetic moments and the projected density of states (Table S1). Clearly, as the concentration of Ni increases from NCM-424 to NCM-811, the concentration of Ni³⁺ ions increases and the concentration of Ni²⁺ decreases (Figure 5a). It is noteworthy that the concentration of Ni⁴⁺ ions as a function of Li content increases more rapidly in Ni-rich materials (NCM-811 and NCM-622), whereas this increase is reduced in the materials with lower Ni content (like NCM-424) (Figure 5b). Recently, Sun et al. estimated the oxidation states of TMs in NCMs based on the TM-O distances.³⁵ They found the existence of Co²⁺ ions along with Co³⁺ ions in pristine NCMs. However, our results (based on magnetic moments and PDOS, see Supporting Information for discussion) indicate that the oxidation state of Co (3+) remains constant in different NCMs in the pristine state. Our results agree with several experimental studies that have confirmed a 3+ Co-oxidation state in different NCMs.^{2,11,15,16,19,44,45,58,70,71} We suspect that for the multi-TM systems (i.e., NCMs), where each oxygen atom shares several different types of TMs, bond distances might not reflect the oxidation states accurately, and the magnetic moments are likely better reporters on oxidation states.

3.3. Chemical Bonding Analysis of NCMs. Chemical bonding plays a primary role in controlling the electrochemical activity and stability of cathode materials. The nature of the chemical bonding between metal and oxygen changes both with the nature of the metal and its oxidation state. To understand the changes in chemical bonding with Ni concentration in

NCMs, we investigated the crystal orbital Hamilton populations (COHP)^{56–58} and the Bader charges.⁷² In Figure 6, we show the chemical bonding descriptors, COHP and integrated COHP (ICOHP) of pristine NCM-811, which we used to examine the M–O bonding with Ni in different oxidation states. ICOHP (up to the Fermi level) indicates that the M–O covalency increases with the oxidation state of Ni. The ICOHP (Figure 6) follows the order Ni²⁺–O (−1.08, −0.64) < Ni³⁺–O (−1.24, −1.13) < Ni⁴⁺–O (−1.34, −1.36), indicating that the covalency of Ni increases with its oxidation states. This conclusion mirrors the one drawn based on the M–O hybridization observed in the DOS above (Figures 3 and 4). The difference in up and down spin ICOHP decreases from Ni²⁺–O to Ni⁴⁺–O due to the reduced number of unpaired electrons at the TM centers. Finally, on comparing the COHP plots with the DOS (Figure 4), we conclude that Ni-t_{2g} has antibonding character.

On the basis of COHP and PDOS (Figures 3, 4, and 6), we constructed a MO diagram for NCM-811 (Figure 7). The diagram was constructed based on an octahedral metal crystal field ligating oxygen.⁷³ In an octahedral field, the oxygen orbitals are split into symmetry adapted $\pi(s-p_z)$ and $\sigma(p_{xy}p_y)$ basis sets. The nature of interactions between metal and oxygen is often ionic due to differences in electronegativity of metal and oxygen, as seen for Ni²⁺ and O²⁻ in Figure 7. However, we note that with an increase in the oxidation states of Ni, the energy difference between the M–O levels decreases due to lowering of the energy of the Ni levels. This effect is clearly seen in Figure 7, where the energy levels of Ni⁴⁺ and O²⁻ are closer in energy, thereby showing pronounced covalency. Experimentally, it has been suggested that Ni⁴⁺–O bonds are unstable and that Ni⁴⁺ is prone to be reduced to its most stable state (Ni²⁺) with concomitant oxygen release. This MO diagram also reveals the possible cause of instability of Ni⁴⁺–O bonds; the Ni⁴⁺–e_g is a very low lying LUMO. This LUMO has significant covalent character and can easily accept electrons from oxygens or the electrolyte at the solid–electrolyte interface.

3.4. Bader Charges and Oxygen Binding Energies.

Atomic charges constitute a metric for understanding the ionic or covalent character of bonds. To further solidify our conclusions regarding increased Ni–O covalency with increasing Ni content in NCMs and on Li deintercalation, we computed the average Bader charges of different NCMs. The average Bader charges on oxygen in NCM-424 and NCM-811 are shown in Figure 8a. We see that the average absolute Bader charge on oxygen atoms linearly decreases with Li deintercalation, indicating an increase in M–O covalency. We also note that the oxygen Bader charges in NCM-811 are consistently lower than NCM-424. Since the average formal charge of the TMs is conserved in NCMs, the reduced Bader charges on oxygen are accompanied by a parallel increase in TM charges, hence indicating an increase in covalency. We therefore conclude that the Bader charges also suggest that the M–O covalency increases with increasing Ni content.

The stability of cathode materials strongly depends on the stability of M–O bonds on Li deintercalation. Since oxygen binding energy is an indicator of the strength of the M–O bonds, we computed the oxygen binding energy as a function of Li content. Inspection of Figure 8b reveals that the oxygen binding energy decreases with increasing Ni content in NCM, as well as with Li deintercalation. The oxygen binding energies were found to decrease with delithiation, but for the fully

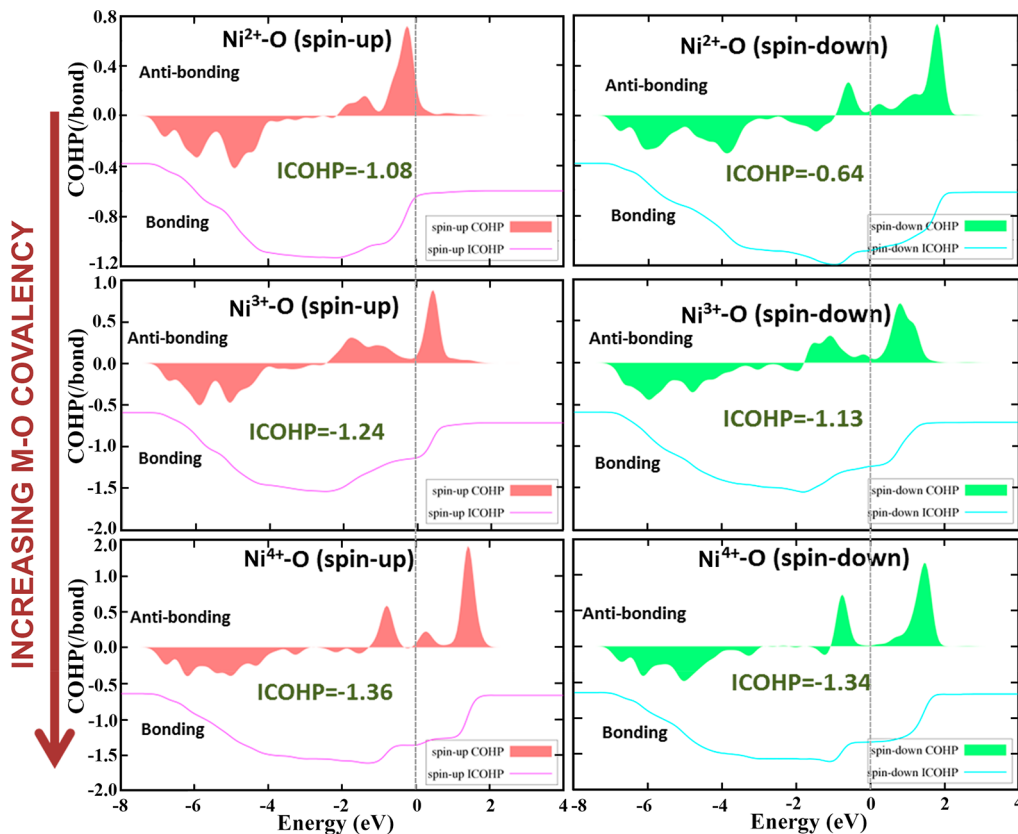


Figure 6. Chemical bonding descriptors, COHP and integrated COHP (ICOHP) for pristine NCM-811.

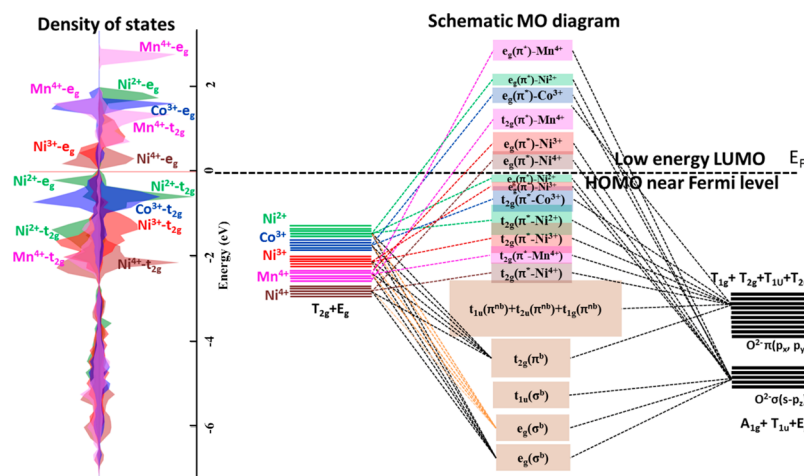


Figure 7. Molecular orbital diagram of NCM-811 based on PDOS and COHP.

delithiated systems, the binding energies increased relative to the corresponding value at $n = 0.75$. We note that for $n = 1.00$ to 0.25, the oxygen release reduces the Ni-ions, but for $n = 0.00$, Co⁴⁺ ions are also reduced along with Ni⁴⁺ ions and the gain in energy for Ni⁴⁺ reduction is different from the gain in energy by the reduction of Co⁴⁺ ions. This is reflected in the increased oxygen binding energies for $n = 0.25$ to $n = 0.00$.

On the basis of the analysis of electronic structure, the COHP and MO diagram above, we suggested that M-O covalency increases with both increasing Ni content and decreasing Li content. One might envision that M-O covalency might lead to stronger M-O bond, but the opposite is true in NCM cathode materials. A high degree of covalency leads to

electron delocalization across the M-O bonds, and during electrochemical oxidation, the M-O bonding electrons are extracted, leading to weakening or rupturing of the M-O bonds.

The decrease in oxygen binding energy with Li deintercalation and with increasing Ni content supports the above findings. Our results show that moving from NCM-424 to NCM-811, or conversely on lithium deintercalation, the oxygen binding energy decreases (i.e., oxygen release is expected to be more rapid). This finding is also mirrored in our computed radial distribution functions (Figures S2–S5). Previous studies on different cathode materials suggested that a higher negative charge on oxygen atoms results in greater oxygen binding energies.^{19,46,74} Herein, we similarly find that the Bader charges

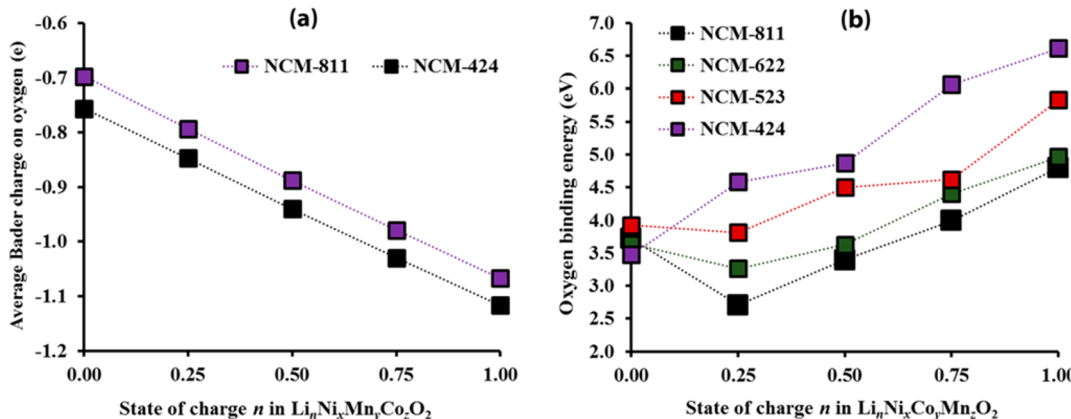


Figure 8. (a) Average Bader charges on oxygen atoms in NCM-424 and NCM-811. (b) Molecular oxygen binding energies for different NCMs as a function of state of charge (Li content).

on oxygen atoms correlate well with oxygen binding energies, indicating that a low charge (i.e., greater covalency) leads to weakening of metal oxygen bonds. Inspection of the electronic and magnetic structure in our oxygen-intact and oxygen-deficient NCM systems shows that Ni^{4+} ions surrounding oxygen sites are reduced to Ni^{2+} states upon oxygen removal, while no change in oxidation states of Co and Mn occurred for $n=1.00$ to $n=0.25$. These results emphasize the tendency of Ni^{4+} to reduce to a Ni^{2+} state, while Co and Mn remain inactive.

3.5. High-Valency Doping in NCM Materials. On the basis of the above analysis, we propose that the oxidation state of Ni-ions plays a primary role for both the electrochemical activity and stability of NCM materials. The Ni^{2+} oxidation state is preferable due to ionic Ni–O interactions and its two redox-active electrons. In contrast, Ni^{4+} is problematic as it leads to Ni–O covalency, and it tends to reduce to Ni^{2+} , via side reactions. On the basis of these findings, we suggest that a high-valent cation doping strategy, which reduces the oxidation state of Ni-ions via charge compensation,⁴⁵ should be a promising direction.^{22,27,46} To demonstrate this, we substituted Mn^{4+} with Nb^{5+} and Mo^{6+} in NCM-622, to generate NCMo-622 and NCNb-622. These *in silico* experiments clearly show that doping with these high valent cations, increases the concentration of Ni^{2+} ions significantly (Table S2).

CONCLUSIONS

It is well-known that the capacity of NCM materials increases with increasing Ni-content, yet the stability in these materials is severely hampered. In the present study, we performed a comparative theoretical analysis of several layered NCM materials to obtain a better understanding of the reason for this reduced stability. Specifically, we employed density functional theory to study structural and electronic properties of NCM-424, NCM-523, NCM-622, and NCM-811. On the basis of extensive analysis of density of states, magnetic structure, bond covalency, molecular orbital diagrams, Bader atomic charges, and oxygen binding energies, we draw several crucial conclusions: as we increase the amount of Ni in NCM materials, (1) the amount of high-valence Ni-ions increases (i.e., N^{3+} , Ni^{4+}), (2) Ni–O bonds become increasingly covalent, as Ni^{4+} -O bonds are more covalent in nature than for Ni in lower oxidation states, (3) Ni^{4+} is readily reduced due to a low-lying LUMO and, hence, can easily react with oxygen or electrolyte species, and (4) molecular oxygen release becomes

more feasible and, hence, results in cathode degradation. Importantly, these conclusions are found to be appropriate also for the deintercalation process for all Ni-rich NCM materials. Hence, a strategy of high-valency doping, which suppresses Ni-ions in high oxidation states via charge compensation, should be adopted. The current results are expected to help in the future rational design of doped NCM and related materials.

ASSOCIATED CONTENT

S Supporting Information

The Supporting Information is available free of charge on the ACS Publications website at DOI: 10.1021/acs.jpcc.7b06122.

Relaxed structures of NCMs, calculated magnetic moments and estimated oxidation states of transition metals in NCMs, calculated radial pair distributed functions for O–O and TM–O pairs in different NCMs, lattice parameters of NCMs at different delithiation levels, method of estimation of oxidation states, and expected electronic structures and schematic projected density states (PDF)

AUTHOR INFORMATION

Corresponding Author

*E-mail: major@biu.ac.il. Tel: + 972 3 531 73 92. Fax: + 972 3 738 40 53.

ORCID

Mudit Dixit: 0000-0001-9456-7806

Doron Aurbach: 0000-0001-8047-9020

Dan T. Major: 0000-0002-9231-0676

Author Contributions

D.T.M. and M.D. designed the research, M.D. performed the studies, and D.T.M., M.D., B.M., F.S., and D.A. wrote the paper.

Notes

The authors declare no competing financial interest.

ACKNOWLEDGMENTS

This work was partially supported by the Israel Science Foundation (ISF) in the framework of the INREP project.

■ REFERENCES

- (1) Etacheri, V.; Marom, R.; Elazari, R.; Salitra, G.; Aurbach, D. Challenges in the Development of Advanced Li-ion Batteries: A Review. *Energy Environ. Sci.* **2011**, *4*, 3243–3262.
- (2) Masquelier, C.; Croguennec, L. Polyanionic (Phosphates, Silicates, Sulfates) Frameworks as Electrode Materials for Rechargeable Li (or Na) Batteries. *Chem. Rev.* **2013**, *113*, 6552–6591.
- (3) Whittingham, M. S. Lithium Batteries and Cathode Materials. *Chem. Rev.* **2004**, *104*, 4271–4302.
- (4) Tarascon, J. M.; Armand, M. Issues and Challenges Facing Rechargeable Lithium Batteries. *Nature* **2001**, *414*, 359–367.
- (5) Bruce, P. G. Energy Storage Beyond the Horizon: Rechargeable Lithium Batteries. *Solid State Ionics* **2008**, *179*, 752–760.
- (6) Goodenough, J. B.; Kim, Y. Challenges for Rechargeable Li Batteries. *Chem. Mater.* **2010**, *22*, 587–603.
- (7) Scrosati, B.; Garche, J. Lithium batteries: Status, Prospects and Future. *J. Power Sources* **2010**, *195*, 2419–2430.
- (8) Islam, M. S.; Fisher, C. A. J. Lithium and Sodium Battery Cathode Materials: Computational Insights Into Voltage, Diffusion and Nanostructural Properties. *Chem. Soc. Rev.* **2014**, *43*, 185–204.
- (9) Dixit, M.; Engel, H.; Eitan, R.; Aurbach, D.; Levi, M. D.; Kosa, M.; Major, D. T. Classical and Quantum Modeling of Li and Na Diffusion in FePO₄. *J. Phys. Chem. C* **2015**, *119*, 15801–15809.
- (10) Osnis, A.; Kosa, M.; Aurbach, D.; Major, D. T. Systematic First-Principles Investigation of Mixed Transition Metal Olivine Phosphates LiM_{1-y}M'_yPO₄ (M/M' = Mn, Fe, and Co) as Cathode Materials. *J. Phys. Chem. C* **2013**, *117*, 17919–17926.
- (11) Meng, Y. S.; Arroyo-de Dompablo, M. E. Recent Advances in First Principles Computational Research of Cathode Materials for Lithium-ion Batteries. *Acc. Chem. Res.* **2013**, *46*, 1171–1180.
- (12) Ohzuku, T.; Makimura, Y. Layered Lithium Insertion Material of LiCo_{1/3}Ni_{1/3}Mn_{1/3}O₂ for Lithium-ion Batteries. *Chem. Lett.* **2001**, *30*, 642–643.
- (13) Belharouak, I.; Sun, Y. K.; Liu, J.; Amine, K. Li(Ni_{1/3}Co_{1/3}Mn_{1/3})O₂ as a Suitable Cathode for High Power Applications. *J. Power Sources* **2003**, *123*, 247–252.
- (14) Liu, W.; Oh, P.; Liu, X.; Lee, M.-J.; Cho, W.; Chae, S.; Kim, Y.; Cho, J. Nickel-Rich Layered Lithium Transition-Metal Oxide for High-Energy Lithium-Ion Batteries. *Angew. Chem., Int. Ed.* **2015**, *54*, 4440–4457.
- (15) Hwang, B. J.; Tsai, Y. W.; Carlier, D.; Ceder, G. A Combined Computational/Experimental Study on LiNi_{1/3}Co_{1/3}Mn_{1/3}O₂. *Chem. Mater.* **2003**, *15*, 3676–3682.
- (16) Noh, H.-J.; Youn, S.; Yoon, C. S.; Sun, Y.-K. Comparison of the Structural and Electrochemical Properties of Layered Li[Ni_xCo_yMn_z]O₂ (x = 1/3, 0.5, 0.6, 0.7, 0.8 and 0.85) Cathode Material for Lithium-ion Batteries. *J. Power Sources* **2013**, *233*, 121–130.
- (17) Armstrong, A. R.; Holzapfel, M.; Novák, P.; Johnson, C. S.; Kang, S.-H.; Thackeray, M. M.; Bruce, P. G. Demonstrating Oxygen Loss and Associated Structural Reorganization in the Lithium Battery Cathode Li[Ni_{0.2}Li_{0.2}Mn_{0.6}]O₂. *J. Am. Chem. Soc.* **2006**, *128*, 8694–8698.
- (18) Hwang, S.; Kim, S. M.; Bak, S.-M.; Cho, B.-W.; Chung, K. Y.; Lee, J. Y.; Chang, W.; Stach, E. A. Investigating Local Degradation and Thermal Stability of Charged Nickel-Based Cathode Materials through Real-Time Electron Microscopy. *ACS Appl. Mater. Interfaces* **2014**, *6*, 15140–15147.
- (19) Nam, K.-W.; Bak, S.-M.; Hu, E.; Yu, X.; Zhou, Y.; Wang, X.; Wu, L.; Zhu, Y.; Chung, K.-Y.; Yang, X.-Q. Combining In Situ Synchrotron X-Ray Diffraction and Absorption Techniques with Transmission Electron Microscopy to Study the Origin of Thermal Instability in Overcharged Cathode Materials for Lithium-Ion Batteries. *Adv. Funct. Mater.* **2013**, *23*, 1047–1063.
- (20) Reed, J.; Ceder, G.; Van Der Ven, A. Layered-to-Spinel Phase Transition in Li_xMnO₂. *Electrochim. Solid-State Lett.* **2001**, *4*, A78–A81.
- (21) Bréger, J.; Meng, Y. S.; Hinuma, Y.; Kumar, S.; Kang, K.; Shao-Horn, Y.; Ceder, G.; Grey, C. P. Effect of High Voltage on the Structure and Electrochemistry of LiNi_{0.5}Mn_{0.5}O₂: A Joint Experimental and Theoretical Study. *Chem. Mater.* **2006**, *18*, 4768–4781.
- (22) Schipper, F.; et al. Stabilizing Nickel-Rich Layered Cathode Materials by a High-Charge Cation Doping Strategy: Zirconium-Doped LiNi_{0.6}Co_{0.2}Mn_{0.2}O₂. *J. Mater. Chem. A* **2016**, *4*, 16073–16084.
- (23) Yang, J.; Xia, Y. Suppressing the Phase Transition of the Layered Ni-Rich Oxide Cathode during High-Voltage Cycling by Introducing Low-Content Li₂MnO₃. *ACS Appl. Mater. Interfaces* **2016**, *8*, 1297–1308.
- (24) Guilmard, M.; Croguennec, L.; Denux, D.; Delmas, C. Thermal Stability of Lithium Nickel Oxide Derivatives. Part I: Li_xNi_{1.02}O₂ and Li_xNi_{0.89}Al_{0.16}O₂ (x = 0.50 and 0.30). *Chem. Mater.* **2003**, *15*, 4476–4483.
- (25) McCalla, E.; et al. Visualization of O-O Peroxo-Like Dimers in High-Capacity Layered Oxides for Li-ion Batteries. *Science* **2015**, *350*, 1516–1521.
- (26) Sathiya, M.; et al. Reversible Anionic Redox Chemistry in High-Capacity Layered-Oxide Electrodes. *Nat. Mater.* **2013**, *12*, 827–835.
- (27) Dixit, M.; Kosa, M.; Lavi, O. S.; Markovsky, B.; Aurbach, D.; Major, D. T. Thermodynamic and Kinetic Studies of Li-Ni_{0.5}Co_{0.2}Mn_{0.3}O₂ as a Positive Electrode Material for Li-ion Batteries Using First Principles. *Phys. Chem. Chem. Phys.* **2016**, *18*, 6799–6812.
- (28) Lee, H.; Kim, Y.; Hong, Y.-S.; Kim, Y.; Kim, M. G.; Shin, N.-S.; Cho, J. Structural Characterization of the Surface-Modified Li_xNi_{0.9}Co_{0.1}O₂ Cathode Materials by MPO₄ Coating (M= Al, Ce, Sr, and Fe) for Li-Ion Cells. *J. Electrochem. Soc.* **2006**, *153*, A781–A786.
- (29) Yun, S. H.; Park, K.-S.; Park, Y. J. The Electrochemical Property of ZrFX-Coated Li[Ni_{1/3}Co_{1/3}Mn_{1/3}]O₂ Cathode Material. *J. Power Sources* **2010**, *195*, 6108–6115.
- (30) Manthiram, A. Materials Challenges and Opportunities of Lithium Ion Batteries. *J. Phys. Chem. Lett.* **2011**, *2*, 176–184.
- (31) Erickson, E. M.; et al. Synthesis and Electrochemical Performance of Nickel-Rich Layered-Structure LiNi_{0.65}Co_{0.08}Mn_{0.27}O₂ Cathode Materials Comprising Particles with Ni and Mn Full Concentration Gradients. *J. Electrochem. Soc.* **2016**, *163*, A1348–A1358.
- (32) Schipper, F.; Erickson, E. M.; Erk, C.; Shin, J.-Y.; Chesneau, F. F.; Aurbach, D. Review—Recent Advances and Remaining Challenges for Lithium Ion Battery Cathodes: I. Nickel-Rich, LiNi_xCo_yMn_zO₂. *J. Electrochem. Soc.* **2017**, *164*, A6220–A6228.
- (33) Erickson, E. M.; Schipper, F.; Penki, T. R.; Shin, J.-Y.; Erk, C.; Chesneau, F.-F.; Markovsky, B.; Aurbach, D. Review—Recent Advances and Remaining Challenges for Lithium Ion Battery Cathodes: II. Lithium-Rich, xLi₂MnO₃ (1-x)LiNi_aCo_bMn_cO₂. *J. Electrochem. Soc.* **2017**, *164*, A6341–A6348.
- (34) Schipper, F.; Nayak, P.; Erickson, E.; Amalraj, S.; Srur-Lavi, O.; Penki, T.; Talianker, M.; Grinblat, J.; Sclar, H.; Breuer, O.; et al. Study of Cathode Materials for Lithium-Ion Batteries: Recent Progress and New Challenges. *Inorganics* **2017**, *5*, 32.
- (35) Sun, H.; Zhao, K. Electronic Structure and Comparative Properties of LiNi_xMn_yCo_zO₂ Cathode Materials. *J. Phys. Chem. C* **2017**, *121*, 6002–6010.
- (36) Kresse, G.; Furthmüller, J. Efficient Iterative Schemes for Ab Initio Total-Energy Calculations Using a Plane-Wave Basis Set. *Phys. Rev. B: Condens. Matter Mater. Phys.* **1996**, *54*, 11169–11186.
- (37) Kresse, G.; Hafner, J. Ab Initio Molecular Dynamics for Liquid Metals. *Phys. Rev. B: Condens. Matter Mater. Phys.* **1993**, *47*, 558–561.
- (38) Kresse, G.; Hafner, J. Ab Initio Molecular-Dynamics Simulation of the Liquid-Metal–Amorphous–Semiconductor Transition in Germanium. *Phys. Rev. B: Condens. Matter Mater. Phys.* **1994**, *49*, 14251–14269.
- (39) Hwang, B. J.; Tsai, Y. W.; Carlier, D.; Ceder, G. A Combined Computational/Experimental Study on LiNi_{1/3}Co_{1/3}Mn_{1/3}O₂. *Chem. Mater.* **2003**, *15*, 3676–3682.
- (40) Chernova, N. A.; Ma, M.; Xiao, J.; Whittingham, M. S.; Breger, J.; Grey, C. P. Layered Li_xNi_yMn_zCo_{1-2y}O₂ Cathodes for Lithium Ion Batteries: Understanding Local Structure via Magnetic Properties. *Chem. Mater.* **2007**, *19*, 4682–4693.

- (41) Yu, H.; Qian, Y.; Otani, M.; Tang, D.; Guo, S.; Zhu, Y.; Zhou, H. Study of the Lithium/Nickel Ions Exchange in the Layered $\text{LiNi}_{0.42}\text{Mn}_{0.42}\text{Co}_{0.16}\text{O}_2$ Cathode Material for Lithium Ion Batteries: Experimental and First-Principles Calculations. *Energy Environ. Sci.* **2014**, *7*, 1068–1078.
- (42) Perdew, J. P.; Burke, K.; Ernzerhof, M. Generalized Gradient Approximation Made Simple. *Phys. Rev. Lett.* **1996**, *77*, 3865–3868.
- (43) Chebiam, R. V.; Prado, F.; Manthiram, A. Soft Chemistry Synthesis and Characterization of Layered $\text{Li}_{1-x}\text{Ni}_{1-y}\text{Co}_y\text{O}_{2-\delta}$ ($0 \leq x \leq 1$ and $0 \leq y \leq 1$). *Chem. Mater.* **2001**, *13*, 2951–2957.
- (44) Julien, C. M.; Mauger, A.; Zaghib, K.; Groult, H. Comparative Issues of Cathode Materials for Li-Ion Batteries. *Inorganics* **2014**, *2*, 132–154.
- (45) Cherkashinin, G.; Motzko, M.; Schulz, N.; Späth, T.; Jaegermann, W. Electron Spectroscopy Study of $\text{Li}[\text{Ni},\text{Co},\text{Mn}]_{\text{O}_2}$ /Electrolyte Interface: Electronic Structure, Interface Composition, and Device Implications. *Chem. Mater.* **2015**, *27*, 2875–2887.
- (46) Dixit, M.; Markovsky, B.; Aurbach, D.; Major, D. T. Unraveling the Effects of Al Doping on the Electrochemical Properties of $\text{LiNi}_{0.5}\text{Co}_{0.2}\text{Mn}_{0.3}\text{O}_2$ Using First Principles. *J. Electrochem. Soc.* **2017**, *164*, A6359–A6365.
- (47) Seo, D.-H.; Urban, A.; Ceder, G. Calibrating Transition-Metal Energy Levels and Oxygen Bands in First-Principles Calculations: Accurate Prediction of Redox Potentials and Charge Transfer in Lithium Transition-Metal Oxides. *Phys. Rev. B: Condens. Matter Mater. Phys.* **2015**, *92*, 115118.
- (48) Park, M. S. First-Principles Study of Native Point Defects in $\text{LiNi}_{1/3}\text{Co}_{1/3}\text{Mn}_{1/3}\text{O}_2$ and Li_2MnO_3 . *Phys. Chem. Chem. Phys.* **2014**, *16*, 16798–16804.
- (49) Radin, M. D.; Van der Ven, A. Stability of Prismatic and Octahedral Coordination in Layered Oxides and Sulfides Intercalated with Alkali and Alkaline-Earth Metals. *Chem. Mater.* **2016**, *28*, 7898–7904.
- (50) Kawasaki, S.; Motohashi, T.; Shimada, K.; Ono, T.; Kanno, R.; Karppinen, M.; Yamauchi, H.; Zheng, G.-q. Measurement of Electron Correlations in Li_xCoO_2 ($x = 0.0–0.35$) Using ^{59}Co Nuclear Magnetic Resonance and Nuclear Quadrupole Resonance Techniques. *Phys. Rev. B: Condens. Matter Mater. Phys.* **2009**, *79*, 220514.
- (51) Mazumdar, S.; Clay, R. T. Is There a Common Theme Behind the Correlated-Electron Superconductivity in Organic Charge-Transfer Solids, Cobaltates, Spinels, and Fullerides? *Phys. Status Solidi B* **2012**, *249*, 995–998.
- (52) Ensling, D.; Thissen, A.; Laubach, S.; Schmidt, P. C.; Jaegermann, W. Electronic Structure of LiCoO_2 Thin Films: A Combined Photoemission Spectroscopy and Density Functional Theory Study. *Phys. Rev. B: Condens. Matter Mater. Phys.* **2010**, *82*, 195431.
- (53) Santana, J. A.; Kim, J.; Kent, P.; Reboledo, F. A. Successes and Failures of Hubbard-Corrected Density Functional Theory: The Case of Mg Doped LiCoO_2 . *J. Chem. Phys.* **2014**, *141*, 164706.
- (54) Laubach, S.; Laubach, S.; Schmidt, P. C.; Ensling, D.; Schmid, S.; Jaegermann, W.; Thißen, A.; Nikolowski, K.; Ehrenberg, H. Changes in the Crystal and Electronic Structure of LiCoO_2 and LiNiO_2 upon Li Intercalation and De-intercalation. *Phys. Chem. Chem. Phys.* **2009**, *11*, 3278–3289.
- (55) Klimeš, J.; Bowler, D. R.; Michaelides, A. Chemical Accuracy for the van der Waals Density Functional. *J. Phys.: Condens. Matter* **2010**, *22*, 022201.
- (56) Drönskowski, R.; Bloechl, P. E. Crystal orbital Hamilton populations (COHP): Energy-Resolved Visualization of Chemical Bonding in Solids Based on Density-Functional Calculations. *J. Phys. Chem.* **1993**, *97*, 8617–8624.
- (57) Deringer, V. L.; Tchougréeff, A. L.; Drönskowski, R. Crystal Orbital Hamilton Population (COHP) Analysis As Projected from Plane-Wave Basis Sets. *J. Phys. Chem. A* **2011**, *115*, 5461–5466.
- (58) Maintz, S.; Deringer, V. L.; Tchougréeff, A. L.; Drönskowski, R. Analytic Projection From Plane-Wave and PAW Wavefunctions and Application to Chemical-Bonding Analysis in Solids. *J. Comput. Chem.* **2013**, *34*, 2557–2567.
- (59) Cahill, L. S.; Yin, S. C.; Samoson, A.; Heinmaa, I.; Nazar, L. F.; Goward, G. R. ^{6}Li NMR Studies of Cation Disorder and Transition Metal Ordering in $\text{Li}[\text{Ni}_{1/3}\text{Mn}_{1/3}\text{Co}_{1/3}]_{\text{O}_2}$ Using Ultrafast Magic Angle Spinning. *Chem. Mater.* **2005**, *17*, 6560–6566.
- (60) Zeng, D.; Cabana, J.; Bréger, J.; Yoon, W.-S.; Grey, C. P. Cation Ordering in $\text{Li}[\text{Ni}_x\text{Mn}_{x}\text{Co}_{(1-2x)}]_{\text{O}_2}$ -Layered Cathode Materials: A Nuclear Magnetic Resonance (NMR), Pair Distribution Function, X-ray Absorption Spectroscopy, and Electrochemical Study. *Chem. Mater.* **2007**, *19*, 6277–6289.
- (61) Weill, F.; Tran, N.; Croguennec, L.; Delmas, C. Cation Ordering in the Layered $\text{Li}_{1+x}(\text{Ni}_{0.425}\text{Mn}_{0.425}\text{Co}_{0.15})_{1-x}\text{O}_2$ Materials ($x = 0$ and 0.12). *J. Power Sources* **2007**, *172*, 893–900.
- (62) Meng, Y. S.; Ceder, G.; Grey, C. P.; Yoon, W. S.; Jiang, M.; Bréger, J.; Shao-Horn, Y. Cation Ordering in Layered O_3 $\text{Li}[\text{Ni}_x\text{Li}_{1/3-2x/3}\text{Mn}_{2/3-x/3}]_{\text{O}_2}$ ($0 \leq x \leq 1/2$) Compounds. *Chem. Mater.* **2005**, *17*, 2386–2394.
- (63) Strobel, P.; Lambert-Andron, B. Crystallographic and Magnetic Structure of Li_2MnO_3 . *J. Solid State Chem.* **1988**, *75*, 90–98.
- (64) Paulsen, J. M.; Dahn, J. R. O₂-Type $\text{Li}_{2/3}[\text{Ni}_{1/3}\text{Mn}_{2/3}]_{\text{O}_2}$: A New Layered Cathode Material for Rechargeable Lithium Batteries II. Structure, Composition, and Properties. *J. Electrochem. Soc.* **2000**, *147*, 2478–2485.
- (65) Aykol, M.; Kim, S.; Wolverton, C. Van der Waals Interactions in Layered Lithium Cobalt Oxides. *J. Phys. Chem. C* **2015**, *119*, 19053–19058.
- (66) Yin, S. C.; Rho, Y. H.; Swainson, I.; Nazar, L. F. X-ray/Neutron Diffraction and Electrochemical Studies of Lithium De/Re-Intercalation in $\text{Li}_{1-x}\text{Co}_{1/3}\text{Ni}_{1/3}\text{Mn}_{1/3}\text{O}_2$ ($x = 0 \rightarrow 1$). *Chem. Mater.* **2006**, *18*, 1901–1910.
- (67) Li, J.; Downie, L. E.; Ma, L.; Qiu, W.; Dahn, J. R. Study of the Failure Mechanisms of $\text{LiNi}_{0.8}\text{Mn}_{0.1}\text{Co}_{0.1}\text{O}_2$ Cathode Material for Lithium Ion Batteries. *J. Electrochem. Soc.* **2015**, *162*, A1401–A1408.
- (68) Ghanty, C.; et al. Li+-Ion Extraction/Insertion of Ni-Rich $\text{Li}_{1+x}(\text{Ni}_y\text{Co}_z\text{Mn}_w)_{\text{O}_2}$ ($0.005 < x < 0.03$; $y:z = 8:1$, $w \approx 1$) Electrodes: In Situ XRD and Raman Spectroscopy Study. *ChemElectroChem* **2015**, *2*, 1479–1486.
- (69) Li, J.; Shunmugasundaram, R.; Doig, R.; Dahn, J. R. In Situ X-ray Diffraction Study of Layered Li–Ni–Mn–Co Oxides: Effect of Particle Size and Structural Stability of Core–Shell Materials. *Chem. Mater.* **2016**, *28*, 162–171.
- (70) Goodenough, J. B.; Park, K.-S. The Li-Ion Rechargeable Battery: A Perspective. *J. Am. Chem. Soc.* **2013**, *135*, 1167–1176.
- (71) Li, J.; Cao, C.; Xu, X.; Zhu, Y.; Yao, R. $\text{LiNi}_{1/3}\text{Co}_{1/3}\text{Mn}_{1/3}\text{O}_2$ hollow nano-micro hierarchical microspheres with enhanced performances as cathodes for lithium-ion batteries. *J. Mater. Chem. A* **2013**, *1*, 11848–11852.
- (72) Tang, W.; Sanville, E.; Henkelman, G. A Grid-Based Bader Analysis Algorithm Without Lattice Bias. *J. Phys.: Condens. Matter* **2009**, *21*, 084204.
- (73) Ballhausen, C. A.; Gray, H. B. *Molecular Orbital Theory: an Introductory Lecture Note and Reprint Vol.*; WA Benjamin, Inc., 1965.
- (74) Xiao, P.; Deng, Z.; Manthiram, A.; Henkelman, G. Calculations of oxygen stability in lithium-rich layered cathodes. *J. Phys. Chem. C* **2012**, *116*, 23201–23204.